A clothing modeling framework for uniform and armor system design

Xiaolin Man[*], Colby C. Swan, Salam Rahmatalla
Dept. of Civil & Environmental Engineering,
Center of Computer-Aided Design,
University of Iowa, Iowa City, IA, USA 52242

ABSTRACT

In the analysis and design of military uniforms and body armor systems it is helpful to quantify the effects of the clothing/armor system on a wearer's physical performance capabilities. Toward this end, a clothing modeling framework for quantifying the mechanical interactions between a given uniform or body armor system design and a specific wearer performing defined physical tasks is proposed. The modeling framework consists of three interacting modules: (1) a macroscale fabric mechanics/dynamics model; (2) a collision detection and contact correction module; and (3) a human motion module. In the proposed framework, the macroscopic fabric model is based on a rigorous large deformation continuum-degenerated shell theory representation. The collision and contact module enforces non-penetration constraints between the fabric and human body and computes the associated contact forces between the two. The human body is represented in the current framework, as an assemblage of overlapping ellipsoids that undergo rigid body motions consistent with human motions while performing actions such as walking, running, or jumping. The transient rigid body motions of each ellipsoidal body segment in time are determined using motion capture technology. The integrated modeling framework is then exercised to quantify the resistance that the clothing exerts on the wearer during the specific activities under consideration. Current results from the framework are presented and its intended applications are discussed along with some of the key challenges remaining in clothing system modeling.

Keywords: fabric modeling, contact, finite element methods, armor design

1. INTRODUCTION

Human beings rely on clothing (a term used herein to include uniforms, body-armor systems, nuclear-biological-chemical war-suits, space suits etc.) for protection against adversities and threats such as cold weather, ballistic projectiles, radiation, chemicals, and biological agents. While clothing systems provide protection it has been well established that they can also adversely impact human mobility and comfort in performing physical tasks. For example, if the clothing binds on the wearer's joints, it can restrict motion or make the performance of necessary tasks much more difficult. Alternatively, if the clothing does not permit heat to be conducted or convected away from the body, the wearer can suffer heat-induced fatigue or stroke. A recent study by Rahmatalla et al. [23] found that the stability of human motion can be significantly affected by clothing restrictions, which eventually cause wearers to change their strategies for accomplishing physical tasks.

Clothing design inevitably involves trial and error until the criteria for both protection and maintained human performance are satisfied. To facilitate this process, it is desirable for clothing system designers to have a modeling tool that can evaluate different designs by quantifying the protection they afford and the impact that they have on human performance. To achieve this goal, it is necessary that the clothing be mathematically characterized and modeled in a way that permits interaction with digital human models. In this paper, a clothing modeling framework, for quantifying the mechanical interactions between a given uniform or body armor system design and a specific wearer performing defined physical tasks is proposed. The modeling framework consists of three interacting modules: (1) fabric mechanics/dynamics modeling; (2) collision detection and contact modeling; and (3) digital human modeling. In the fabric mechanics/dynamics module, two alternative approaches are described: the first is a particle-based method that models the fabric as a system of springs and masses, and the second is a nonlinear shell theory treatment based on

---

[*] xman@engineering.uiowa.edu; phone 1 319 335 5614; fax 1 319 384 0542

continuum mechanics and dynamics. The collision and contact module enforces non-penetration constraints between the clothing system and digital human models and computes the mutual contact forces between the two. While the human modeling module might eventually include intelligent and autonomous digital human models, the human models in this study are generated by treating the body as a system of rigid ellipsoids whose dynamic motion is driven by motion capture data. Putting the entire framework together, the clothing is first draped onto the human model's form. Then, as the human form goes through its prescribed motions, the contact forces between the draped clothing and the model are computed. These contact forces quantities are then integrated over space and time to quantify the resistance that the closing exerts on the wearer during the specific activity considered.

2. REVIEW

Fabrics are very flexible materials and form complex drape configurations with unfathomable wrinkling patterns. It has always been a challenge to replicate these seemingly disordered drapes. And it poses an even challenging problem to make sense out of the disorder and to understand the mechanics governing it. In this section, some representative works on fabric modeling are summarized and based on their formulations these works are broadly grouped into two types: particle-based method and surface-based method.

2.1. Particle-based method

Particle-based method treats fabrics as a dynamic system composed of interacting mass points or particles and solves cloth draping or deformation by time integration of the system. Simple as it is, the method can generate realistic cloth animations and has been widely applied in computer graphics.

A pioneering work is the mass-spring cloth model proposed by Provot [22]. In his model, fabric is modeled as an array of mass particles inter-connected by linear springs of three different types, structural, shear and flexion springs (Fig.1), which characterizes the stretching, in-plane shear and bending behaviors respectively. Structural springs connect a particle with its direct neighbors along the two perpendicular axes, which are usually aligned with warp and weft yarn directions, while shear springs connect a particle with its neighbors in the diagonal directions. Flexion springs are also along the two perpendicular yarn axes but each connects every other particles. Cloth drape is solved by an explicit time integration of the system. Since the step size of the integrator is limited by the spring stiffness, compliant springs were used, which resulted in some unrealistic overstretching. To address this issue, a heuristic method was proposed by Provot to adjust the positions of the particles associated with the overstretched springs. An extension of the mass-spring model was proposed by Choi and Ko[9] in 2002. They considered fabric buckling and included it in the formulation of the bending springs. In their model, a bending spring is treated as a buckling column with both ends pinned and a nonlinear force-compression relation was derived.
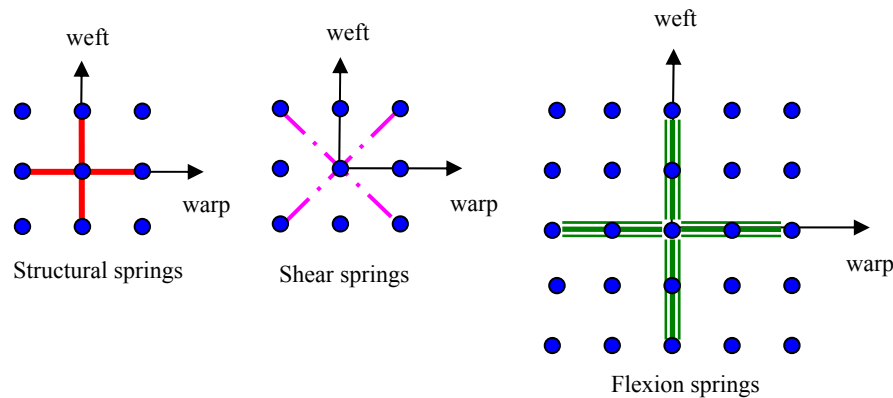

Figure 1: A mass-spring model by Provot

Breen et al. [4, 5] considered incorporation of experimental results into their particle model. In their model, four basic mechanical interactions between particles, i.e. repulsion, stretching, bending and in-plane shear, were defined using energy functions and fabric drape was found by minimizing the strain energy of the whole system. The energy functions of bending and in-plane shear were based on experimental data obtained from Kawabata Evaluation System

for Fabrics (KES-F) [20]. As the internal forces between particles can be derived by taking the derivatives of the energy functions, the model can be reformulated as a generalized mass-spring model with nonlinear internal forces. Motivated by Breen et al.'s work, Eberhardt et al. [13] proposed a model to simulate the dynamics of fabric draping. The Lagrange equation governing particle trajectory was considered and differentiated symbolically. The resulting differential equations were solved by a Runge-Kutta method with adaptive step-size control. The strain energy functions for bending and in-plane shear were based on experimental data and fabric hysteresis was included by constructing piecewise linear approximation to experiment curves.

These works among others, which are not cited in this paper, generate visually realistic draping configurations and shed light on the puzzle of fabric modeling. However, most particle models fall short in presenting an explicit definition on the discretization technique, which transforms a real fabric surface into a computation model of springs or coupling particle pairs. A particle model in theory is a "fishnet"-like representation of a fabric surface and the bridging between the two depends on a specification of the discretization. The vague definition introduces difficulties in transferring information between the two. For example, how to determine spring stiffness for a given fabric and how to find the stress in a fabric patch based on the spring force. Ad-hoc assumptions have to be made to answer these questions. In this sense, particle-based method is not rigorous unless an explicit discretization is specified.

2.2. Surface-based methods

Unlike particle-based method, surface-based method considers the local equilibrium of a continuum and uses that as a point of depart. Models are derived following standard computational techniques, such as finite difference methods or finite element methods. The surface-based method is generally more rigorous in a mathematical and mechanical sense because the discretization procedure is explicitly specified. However, it is usually more complex than the particle-based method.

In order to create animations of deformable bodies in computer graphics, Terzopoulos et al. [32] introduced a physically-based model by applying the principles of elasticity and differential geometry. They started with the local form of Lagrange equation and adopted metric tensors derived from differential geometry as strain measures. The constitutive functions were then derived based on strain energy functions. The governing equation was discretized by finite difference methods over a regular mesh. A set of second-order ordinary differential equations was obtained and solved by implicit time integration. Their model is quite general, which includes the deformation of curves, surfaces and solids. In one of their later work, Terzopoulos and Fleischer [33] even included viscoelasticity, plasticity and fracture into their model, enabling a complete physical-based simulation framework for computer graphics. Terzopoulos's general model was extended by Carignan et al. [6] for cloth simulation and some great work on garment and virtual human simulation has be conducted by their group, which is currently known as Miralab.

In 1991, Collier et al [11] showed that fabric drape can be predicted using a nonlinear shell finite element model. A circular piece of cotton plain-weave fabric was modeled and the drape predicted by the model was compared with experimental results of drape test [10, 12]. A four-node quadrilateral flat-shell element, which combines a membrane element with a plate-bending element, was adopted and Green strain measure was used. Two constitutive models, isotropic and orthotropic linear elasticity were tested and it was found out that the orthotropic one is more appropriate for fabric modeling. Three input parameters were needed for the orthotropic model, the tensile moduli in two yarn family directions, which were measured using KES-F system, and the Poisson's ratio, for which literature values were used. An interesting effect was reported that the deformed shape was sensitive to the Poisson's ratio.

In the mid 90s, Chen and Govindaraj [7, 8] proposed a fabric model based on biquadratic degenerated continuum shell elements. The constitutive relationship used to represent the fabric was orthotropic linear elasticity in which the Young's moduli and the shear moduli were obtained by KES-F and the Poisson's ratio was determined from tests using an Instron tensile tester. Nonlinear strain measures defined in local curvilinear coordinate frames were adopted and a Newton-Raphson method was used to solve the nonlinear equations. Fabric drape shapes predicted by the model were compared with the actual experiment measurements and good agreements were observed. In addition, Chen and Govindaraj [8] did some parametric studies of the effects of various material properties on the drape deformation. It was found that orthotropy in drape deformations were affected by the thickness and shear modulus. For low shear modulus or small thickness, the model didn't exhibit orthotropic drape shapes even though orthotropic material properties were used. Poisson's ratio didn't affect the drape shape, which is contrary to what has been reported by

Collier et al. [11]. Moreover, they presented an example showing that Young's and shear moduli retrieved in the low strain range of Kawabata experiment data generated drape shape very close to actual one, which indicated that for fabric drape linear elastic model is an acceptable assumption.

Around the same time, Gan et al [16] reported a geometrically nonlinear implicit shell fabric model based on the curved degenerated shell element of Bathe [1]. Green strain and Piola-Kirchhoff stress were used to describe the strains and stresses and the problem was solved using Newton-Raphson method. They assumed that fabrics are linearly elastic and orthotropic. Instead of relating the bending stiffness of fabrics to the Young's moduli based on linear strain assumption as Chen and Govindaraj did, they assumed that fabrics have independent bending and tensile stiffness and experimental data of fabric bending rigidity obtained from KES-F system were used. In order to eliminate locking, reduced integration with zero energy mode control was applied. Two examples were presented, one simulating two-dimensional cantilever bending and the other simulating three-dimensional drape. The simulation results were checked against experimental measurements and good agreement was found.

Deviating from traditional degenerated shell elements, Eischen [14] proposed a fabric model based on Simo's [25,26, 27] geometrically exact shell theory. Isotropic elastic material model with a nonlinear moment/curvature relationship derived from KES-F system was used and arc-length controlled solution technique was implemented to treat the instability due to fabric buckling. The contact between fabrics and rigid surfaces was considered and the contact constraint was enforced by a penalty method. Examples such as fabric drape and handing were presented.

3. CLOTHING MODELING FRAMEWORK

3.1. Fabric modeling module

As reviewed in the previous section, two major approaches are available for fabric modeling. In this work, both approaches have been implemented and studied. First a particle model is constructed and it follows mostly Provot's work [22] with three types of linear springs (Fig.1) and viscous damping added to introduce some internal energy dissipation. This framework was implemented with an explicit forward Euler time integration scheme. In the following, a finite element model based on rigorous nonlinear continuum shell theory is presented.

3.1.1. Nonlinear shell finite element formulation

The governing continuum equations of motion in a Lagrangian description can be written as follows, using standard continuum mechanics notation [e.g. Eringen, 15]:

$$P_{Ji,J} + \rho_0 b_i = \rho_0 \ddot{u}_i \ \forall \mathbf{X} \in \Omega_0 \tag{1}$$

where Ω_0 is the reference configuration and P_{Ji} is the first Piola-Kirchhoff stress tensor. If tractions $\bar{t}_i^0$ are applied to the system on $\Gamma_{t_i}^0$, then $n_J^0 P_{Ji} = \bar{t}_i^0$ thereon. Furthermore, if prescribed displacements are applied to the system on $\Gamma_{u_i}^0$ then $u_i = \bar{u}_i$ thereon. Introducing a kinematically admissible variational displacement field $\delta\mathbf{u}$ on Ω_0, the weak form corresponding to Eq. (1) is obtained as

$$\int_{\Omega_0} \delta u_{i,J} P_{Ji} d\Omega_0 = \int_{\Omega_0} \delta u_i \rho_0 b_i d\Omega_0 + \int_{\Gamma_{t_i}^0} \delta u_i \bar{t}_i^0 d\Gamma_0 - \int_{\Omega_0} \delta u_i \rho_0 \ddot{u}_i d\Omega_0 \ . \tag{2}$$

The left-hand side of the preceding is the virtual work done by internal stresses, which is denoted as δW^{int}, and it could be verified that

$$\delta W^{int} = \int_{\Omega_0} \delta F_{iJ} P_{Ji} d\Omega_0 = \int_{\Omega_0} \tfrac{1}{2} \delta C_{IJ} S_{IJ} d\Omega_0 \ , \tag{3}$$

where: $F_{ij} = x_{i,J}$ is the deformation gradient; $C_{IJ} = F_{kI}F_{kJ}$ is the right-Cauchy-Green deformation tensor, and $S_{IJ} = P_{Ik}F_{Jk}^{-1}$ is the 2nd Piola-Kirchhoff stress tensor which is symmetric.

The geometrical description of a shell, following Hughes [19], has the initial global position vector of a material point (ξ, η, ζ) in a shell element is defined by the following interpolation:

$$\mathbf{X}(\xi, \eta, \zeta) = \sum_{A=1}^{nen} N_A(\xi, \eta)\overline{\mathbf{X}}_A + \sum_{A=1}^{nen} N_A(\xi, \eta)z_A(\zeta)\hat{\mathbf{X}}_A \,, \tag{4}$$

where in accordance with Figure 2, $\overline{\mathbf{X}}_A$ is the initial position vector of node A; $\hat{\mathbf{X}}_A$ is the fiber director emanating from node A in the fiber direction; $z_A(\zeta)$ is a thickness function; $N_A(\xi, \eta)$ denotes a two-dimensional shape function associated with node A and nen is the number of element nodes. At each node a local fiber coordinate system $\left(\mathbf{e}_{A1}^f, \mathbf{e}_{A2}^f, \mathbf{e}_{A3}^f\right)$ is constructed and nodal rotations are specified with respect to the frame. In the initial configuration $\mathbf{e}_{A3}^f$ is chosen to coincide with the fiber direction $\hat{\mathbf{X}}_A$ and the other two legs are constructed using the algorithm given in [19].
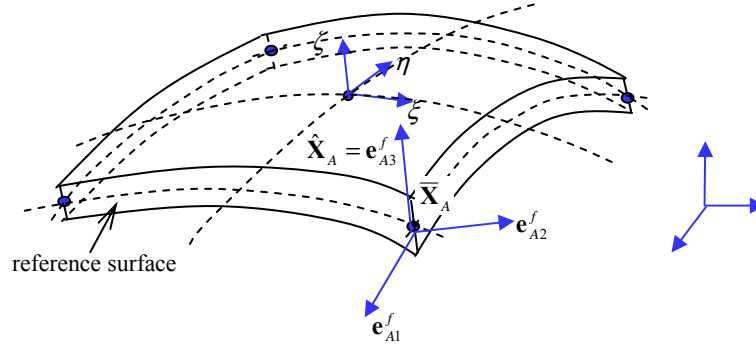

Figure 2: Geometrical description of the shell element

The updated configuration of the shell is defined in a similar manner

$$\mathbf{x}(\xi, \eta, \zeta) = \sum_{A=1}^{nen} N_A(\xi, \eta)\overline{\mathbf{x}}_A + \sum_{A=1}^{nen} N_A(\xi, \eta)z_A(\zeta)\hat{\mathbf{x}}_A \,, \tag{5}$$

where $\overline{\mathbf{x}}_A$ and $\hat{\mathbf{x}}_A$ denote the current nodal position and fiber orientation, respectively. For finite deformation, these nodal quantities are related to the initial ones as

$$\overline{\mathbf{x}}_A = \overline{\mathbf{X}}_A + \overline{\mathbf{u}}_A \text{ and } \hat{\mathbf{x}}_A = \mathbf{R} \cdot \hat{\mathbf{X}}_A \tag{6}$$

where $\overline{\mathbf{u}}_A$ denotes the nodal translation and $\mathbf{R}$ is an orthogonal transformation describing a finite rotation of the nodal fiber director. As Eq. (6) suggests, the vector $\hat{\mathbf{x}}_A$ is obtained by rotating $\hat{\mathbf{X}}_A$ by an angle θ about an axis defined by unit vector $\mathbf{n}$. According to Euler's theorem, the rotation matrix in Eq. (6) can be written as

$$\mathbf{R}(\boldsymbol{\theta}) = \mathbf{I} + \frac{\sin\theta}{\theta}\boldsymbol{\Omega}(\boldsymbol{\theta}) + \frac{1-\cos\theta}{\theta^2}\boldsymbol{\Omega}^2(\boldsymbol{\theta}) \,, \tag{7a}$$

with

$$\boldsymbol{\Omega}(\boldsymbol{\theta}) = \begin{bmatrix} 0 & -\theta_3 & \theta_2 \\ \theta_3 & 0 & -\theta_1 \\ -\theta_2 & \theta_1 & 0 \end{bmatrix} \text{ and } \theta = (\boldsymbol{\theta} \cdot \boldsymbol{\theta})^{1/2} \,. \tag{7b}$$

In shell kinematics, nodal rotations are permitted about the first two axes of the fiber basis (e.g. $\boldsymbol{\theta} = \theta_{A1}\mathbf{e}_{A1}^f + \theta_{A2}\mathbf{e}_{A2}^f$), which excludes the drilling degree of freedom about $\mathbf{e}_{A3}^f$, and the new orientation of fiber director $\hat{\mathbf{X}}_A$ is thus given by

$$\hat{\mathbf{x}}_A = \hat{\mathbf{X}}_A + \frac{\sin\theta}{\theta}\left(\theta_{A2}\mathbf{e}_{A1}^f - \theta_{A1}\mathbf{e}_{A2}^f\right) + \left(1 - \cos\theta\right)\mathbf{e}_{A3}^f . \tag{8}$$

The fiber director tip, i.e. $\hat{\mathbf{u}}_A = \hat{\mathbf{x}}_A - \hat{\mathbf{X}}_A$, is

$$\hat{\mathbf{u}}_A = \frac{\sin\theta}{\theta}\left(\theta_{A2}\mathbf{e}_{A1}^f - \theta_{A1}\mathbf{e}_{A2}^f\right) + \left(1 - \cos\theta\right)\mathbf{e}_{A3}^f , \tag{9}$$

which recovers the infinitesimal rotation case $\hat{\mathbf{u}}_A = \theta_{A2}\mathbf{e}_{A1}^f - \theta_{A1}\mathbf{e}_{A2}^f$ given in [19] when $\theta \to 0$.

Considering the shell kinematic relations of Eqs. (4)-(7), the shell configuration is a nonlinear function of nodal translations and rotations, which can be written in abstract form as $\mathbf{x} = \mathbf{x}(\mathbf{d}_A)$ with nodal displacement vector defined as $\mathbf{d}_A = \left(\bar{u}_{A1}, \bar{u}_{A2}, \bar{u}_{A3}, \theta_{A1}, \theta_{A2}\right)^T$. The variation of the updated shell configuration can be written as

$$\delta x_i = H_{i\chi}^A \delta d_{A\chi}, (\chi = 1,2,\ldots 5) . \tag{10}$$

3.1.2. Constitutive model

In general, fabrics are structures of yarns of two families, i.e. warp and weft, woven together following certain weave patterns. Many factors, such as the constituent yarn properties, the weave patterns, the geometry of yarn structures and the interactions of interwoven yarns, affect the overall material properties of fabrics. As a result, the material properties of fabrics are extremely complex. Nonlinearity, anisotropy and hysteresis are generally observed. A typical load-stretch curve of a biaxial extension test of fabrics is shown in Fig.3a, which can usually be obtained by Kawabata Evaluation System for Fabrics (KES-F) [20]. The initial part of the curve is relatively compliant and it corresponds to yarn decrimping, i.e. the curvatures of yarns decreasing as the yarns are being straightened by tension. Then the fabric shows much stiffer responses as the yarns are actually stretched after they have been straightened. In addition, since the numbers of yarns of the two families and their configurations are usually different, the tensile behaviors of the warp and weft directions differ and exhibit anisotropy. Fabrics also exhibit hysteresis. A load-deformation curve of a fabric bending test is sketched in Fig.3b, from which one may notice that energy is dissipated when the fabric is subjected to a loading and unloading loop. Similar behavior can also be observed in the in-plane shear test as shown in Fig.3c. The dissipative feature of fabrics is due to the frictions between and within yarns. From Fig.3c, one may also notice that fabrics become stiffer when the shear angles increase. This is due to a phenomenon called locking, where yarns jam against each other and further loading induces deformation of yarns' cross sections.
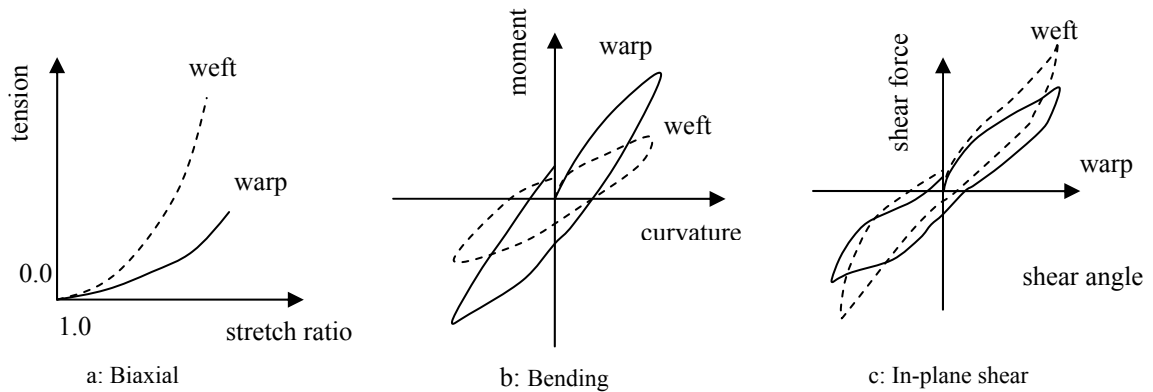

Fig.3: Material properties of fabrics

To capture the complex fabric behaviors, mesoscale models with a resolution where yarn interaction is visible are needed and computational homogenization techniques such as Swan et al. [31] should be utilized. Currently research on

this multiscale fabric modeling is being actively pursued by the authors. In this work, however, hyperelastic constitutive models, which are based on some simplifying assumptions yet amenable to the shell formulation, are adopted. For hyperelastic materials, a strain energy function $\psi(\mathbf{C})$ exists and the second Piola-Kirchoff stress tensor $\mathbf{S}$ and the associated tangent elasticity tensor $\mathbf{D}$ can be derived from it as follows:

$$\mathbf{S} = 2\frac{\partial \psi(\mathbf{C})}{\partial \mathbf{C}}; \quad \mathbf{D} = 4\frac{\partial^2 \psi}{\partial \mathbf{C}\partial \mathbf{C}} \tag{11}$$

The tangent elasticity tensor $\mathbf{D}$ relates the change of $\mathbf{S}$ to that of $\mathbf{C}$ as $d\mathbf{S} = \frac{1}{2}\mathbf{D} : d\mathbf{C}$. Different definitions of the strain energy function $\psi(\mathbf{C})$ can model materials varying from isotropic elasticity to fiber-reinforced composites (Spencer [29]). For problems involving large displacements/rotations yet small strains, St. Venant model provides a good approximation. The model, which is a simple extension of linear elasticity, is as follows

$$\mathbf{S} = \frac{1}{2}\mathbf{D} : (\mathbf{C} - \mathbf{I}). \tag{12}$$

By assuming that under normal wearing conditions the strains in fabrics are small and linear, the model is used as a placeholder for the constitutive model of the fabric modeling module. The St. Venant model can feature anisotropy and can be easily incorporated in the nonlinear shell formulation.

Most shell theories enforce the so-called vanishing normal stress condition, which requires that the normal stress component acting on a lamina surface vanishes. To enforce the constraint for general material models can be a nontrivial endeavor (Swan and Cakmak, [30]), and so a corotational lamina basis is usually constructed at each quadrature points such that one base vector say $\mathbf{e}^l_3$ is always orthogonal to the other two $\mathbf{e}^l_1$ and $\mathbf{e}^l_2$ as shell deforms, and the Cauchy stress component $\sigma^l_{33}=0$ is invoked to condense the material tangent moduli ([19], [2]). In this work, a similar approach is adopted but formulated using a Lagrangian description. A lamina basis $\mathbf{E}^l_I$, (I=1,2,3) is constructed at each quadrature point in the reference configuration and the vanishing normal stress condition is specified in terms of the 2$^\text{nd}$ Piola-Kirchhoff stress as $S^l_{33}=0$, which in general is different from $\sigma^l_{33}=0$ unless the lamina normal remains normal after deformation, i.e. $\mathbf{F}\cdot\mathbf{E}^l_3$ coincides with $\mathbf{E}^l_3$. For thin fabrics transverse shear is negligible and the condition $S^l_{33} = 0$ closely enforces the vanishing normal stress constraint.

3.1.3. Solution algorithm

With finite element interpolation in (5) the weak form of the equation of motion can be transformed into a system of discrete nonlinear at a given time $t \in [0,T]$

$$\mathbf{r} = \mathbf{f}^{int} - \mathbf{f}^{ext} + \mathbf{M}\cdot\mathbf{a} = \mathbf{0}, \tag{13}$$

where $\mathbf{f}^{int}$ and $\mathbf{f}^{ext}$ are the internal and external force vectors, respectively, arising from the left and right sides of Eq. (6) and the term $\mathbf{M}\cdot\mathbf{a}$ is the inertial force vector. Specific expressions for the internal and external force vectors acting on a node A in the model are given as follows:
where

$$f^{int}_{A\chi} = \int_{\Omega_0} H^A_{k\chi,I} F_{kJ} S_{IJ} d\Omega_0 \quad \text{and} \quad f^{ext}_{A\chi} = \int_{\Omega_0} H^A_{i\chi}\rho_0 b_i d\Omega_0 + \int_{\Gamma^0_{t_i}} H^A_{i\chi}\bar{t}^0_i d\Gamma_0 \, , (\chi = 1,2,\ldots,5) \tag{14}$$

For quasi-static problems, the inertial forces can be neglected although in clothing system modeling, inclusion of such effects tends to increase the robustness of the framework. When clothing is modeled quasi-statically by neglecting inertial terms, buckling and wrinkling instabilities of the fabric create numerical instabilities. Although continuation techniques (Riks [24]) can help carry the analysis through points of instability, the robustness of the method is still inadequate. Hence, it is generally best to solve the clothing modeling problems as dynamics problems since the mass matrix helps maintain a positive definite tangent operator and stabilizes the system. Newmark's time-integration method (Hughes [19]) is used to advance the solution in time. Within the Newmark integration method, both explicit and implicit time integration algorithms can be used with appropriate selection of the two integration parameters. The pros and cons of the implicit and explicit time-integration schemes have been well studied in literatures (Belytschko et al. [2]) their discussion here is not necessary. However, one observation is that when contact computation is included in fabric modeling, the time step size of an implicit solution scheme may need to be reduced in order to maintain an

effective tangent operator, which sometimes makes an explicit integrator a better choice. Such a situation is analogous to automotive crash simulations where explicit solvers dominate.

3.2. Collision detection and contact computation module

This module enforces the non-penetration constraint between clothing and a human model and computes the mutual contact forces between the two. Collision detection identifies the penetration of a node or a particle into a surface. Depending on the geometric representations, the expense of collision detection varies significantly. The most general case would be identifying collision between two polygonal meshes, like two finite element meshes. A brute force method searches each potential pairs with a complexity of $O(N^2)$, where N is the number of polygons in a mesh. If relative sliding of the two parts is small, locality can be utilized to reduce the expense by lower the number of candidate pairs (Hallquist et al. [18]). However, such techniques are not applicable to clothing modeling as wrinkling breaks the locality assumption (Benson et al. [3]) and this very reason makes collision detection for self-contact very challenging. Govindaraju et al. [17] presented a novel collision detection algorithm for complex deformable models and achieved interactive rates.

In this work, collision detection is limited to clothing with human model represented by implicit surfaces, which are defined by scalar functions with penetration identifiable by simple function evaluation. Considering an implicit surface defined as $f(\mathbf{x}) = 0$, if a spatial point $\mathbf{x}$ is inside the region enclosed by the surface, then $f(\mathbf{x}) < 0$. Otherwise, $f(\mathbf{x}) \geq 0$. An example of implicit surfaces is an ellipsoid whose surface is defined by Eq. (15). If the human body is modeled as an assemblage of ellipsoids rather than surface polygons, the cost for collision detection is greatly reduced.

$$f(\mathbf{x}) = \sum_{i=1,2,3} \left[\left(x_i - x_i^c \right)^2 / r_i^2 \right] - 1 = 0 \tag{15}$$

Once collision is detected, the clothing points that have penetrated the body must be returned to the surface of the body which requires position, velocity and acceleration adjustment of the penetrating node/particle and also computation of the nodal contact force. There are two approaches for contact computation: explicit and implicit contact solution algorithm. An explicit contact algorithm corrects the state of a penetrating node/particle based on the current state and equilibrium condition at next time step is not considered. An example is the hydrocode slideline methodology, which was summarized and extended by Hallquist et al. [18]. An implicit contact solution algorithm is formulated such that the equilibrium at the end of a time increment is satisfied. An example is the continuum-based formulation for multi-body contact problems proposed by Simo and Laursen [21,28]. Explicit contact solution algorithms are usually more robust but suffer from lower accuracy. While for an implicit contact algorithm, as linearization is necessary, the convergence may be affected by the discontinuities in contact conditions.

In this work, an explicit contact algorithm based on rigid ellipsoidal surfaces is employed. The algorithm works as follows: (1) The position and velocity of a penetrating node/particle are modified using closet projection and non-resilient impact assumptions; (2) The residual force on the node/particle is then computed and the contact force is determined based on the contact conditions. To illustrate, suppose the location and the velocity of a particle are given by $\mathbf{x}$ and $\mathbf{v}$, respectively and the outward normal of the contact surface at $\mathbf{x}$ is denoted as $\mathbf{n}$. The residual force $\mathbf{F}$, which excludes the possible contribution from the contact surface, can be expressed as $\mathbf{F} = \mathbf{F}_N + \mathbf{F}_T$, with $\mathbf{F}_N = (\mathbf{F} \cdot \mathbf{n})\mathbf{n}$ and $\mathbf{F}_T = \mathbf{F} - \mathbf{F}_N$. Likewise, the velocity is also decomposed into tangential and normal components as $\mathbf{v} = \mathbf{v}_N + \mathbf{v}_T$. Since the particle is not allowed to penetrate the surface, $v_N = 0$, if $v_N < 0$. The contact force is determined as follows:

$$\begin{aligned}
&\text{If } \mathbf{F} \cdot \mathbf{n} > 0, \text{ then } \mathbf{f} = 0, \text{ i.e. contact open;} \\
&\text{If } \mathbf{F} \cdot \mathbf{n} < 0 \text{ and } |\mathbf{v}_T| = 0 \text{ and } |\mathbf{F}_T| < \mu_s |\mathbf{F}_N|, \text{ then } \mathbf{f} = -\mathbf{F}; \\
&\text{If } \mathbf{F} \cdot \mathbf{n} < 0 \text{ and } |\mathbf{v}_T| = 0 \text{ and } |\mathbf{F}_T| > \mu_s |\mathbf{F}_N|, \text{ then } \mathbf{f} = -\mathbf{F}_N - \mu_s |\mathbf{F}_N| \mathbf{F}_T / |\mathbf{F}_T|; \\
&\text{If } \mathbf{F} \cdot \mathbf{n} < 0 \text{ and } |\mathbf{v}_T| > 0, \text{ then } \mathbf{f} = -\mathbf{F}_N - \mu_k |\mathbf{F}_N| \mathbf{v}_T / |\mathbf{v}_T|,
\end{aligned} \tag{16}$$

where μ_s and μ_k denote the static and kinetic frictional coefficient, respectively.

3.3. Human motion module

The human model is grossly represented by an assemblage of rigid ellipsoids and the kinematics data of human motion are collected using motion capture to record the motion of each ellipsoidal segment. As each ellipsoid is treated as a rigid entity, the space it occupies at any instant in time is determined by the location of the centroid and the orientation of the ellipsoid. This information is provided by determining the location history of two joint diametrically opposed points $\mathbf{J}_1$ and $\mathbf{J}_2$, and the location history of an auxiliary marker position $\mathbf{M}$. The centroid and the orientation basis of the ellipsoid at any instant in time are then constructed as follows

$$\text{center: } \mathbf{x}^c = \frac{1}{2}\left(\mathbf{J}_1 + \mathbf{J}_2\right); \tag{17a}$$

$$\text{orientation: } \hat{\mathbf{e}}_1 = \frac{\mathbf{J}_2 - \mathbf{J}_1}{\left|\mathbf{J}_2 - \mathbf{J}_1\right|}; \quad \hat{\mathbf{e}}_2 = \frac{\left(\mathbf{M} - \mathbf{x}^c\right) - \left[\left(\mathbf{M} - \mathbf{x}^c\right)\cdot\hat{\mathbf{e}}_1\right]\hat{\mathbf{e}}_1}{\left\|\left(\mathbf{M} - \mathbf{x}^c\right) - \left[\left(\mathbf{M} - \mathbf{x}^c\right)\cdot\hat{\mathbf{e}}_1\right]\hat{\mathbf{e}}_1\right\|}; \quad \hat{\mathbf{e}}_3 = \hat{\mathbf{e}}_1 \times \hat{\mathbf{e}}_2. \tag{17b}$$

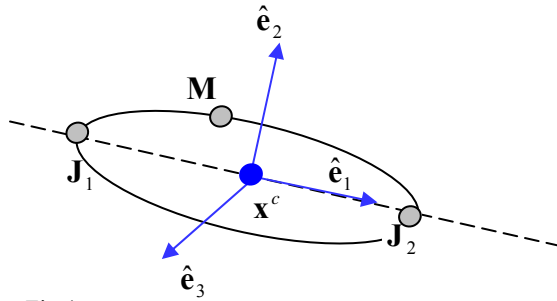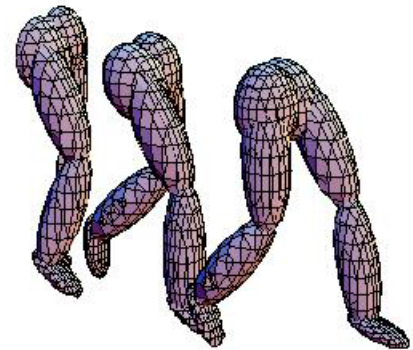Fig.4a: Fig.4b:

Figure 4. Representation of the human body with an assemblage of ellipsoids. a) re-constructing the motion of each ellipsoid using motion capture data that records for each ellipsoid the position histories of points $\mathbf{J}_1$, $\mathbf{J}_2$, and $\mathbf{M}$.; and b) a lower body walking model.

4. RESULTS

4.1. Shell implementation validation

The large-deformation behavior of the shell element implemented for this clothing modeling framework has been tested on a number of problems and performed very well. One such example problem is the beam roll-up problem in which a monotonically increasing bending moment is applied to the free end of the beam, causing it to roll-up as shown in Fig. 5. To test the shell element under dynamic contact conditions, a square patch of fabric pinned at one corner was draped onto an ellipsoid as shown in Fig. 6. Convergence of the draping results was found with refinement of both the spatial discretization of the mesh, and the analysis time-step.
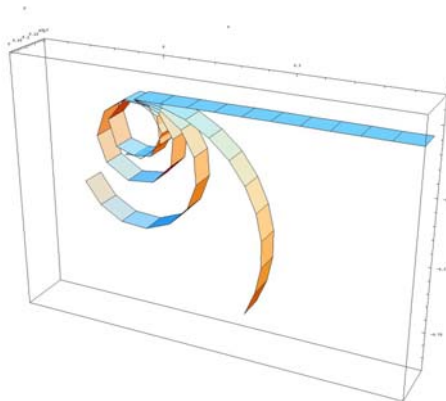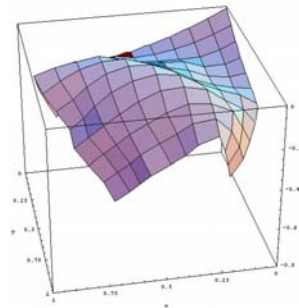

Fig.5: Shell roll-up problem   Fig.6: Fabric shell draping problem

4.2. Pants simulation on walking legs

In this problem, a human subject walked four strides, with the third involving stepping over an obstacle 0.5m in height. The motion of this human was captured with an array of eight infrared Vicon cameras, and the motions were then mapped onto the assemblage of ellipsoids (Fig. 4b) to make them walk. A pair of pants was then placed onto the human model (Fig. 7) in the following sequence: (a) the feet of the human model were removed; (b) the pants of were pulled up over the legs and pelvis; (c) the feet of the human model were then restored; and (d) the effect of a belt was created by tensioning the fabric at the waistline. With the garment on the human model, a simulation of the interaction between the pants and the walking lower body walking and crossing the obstacle was then undertaken (Fig. 8).
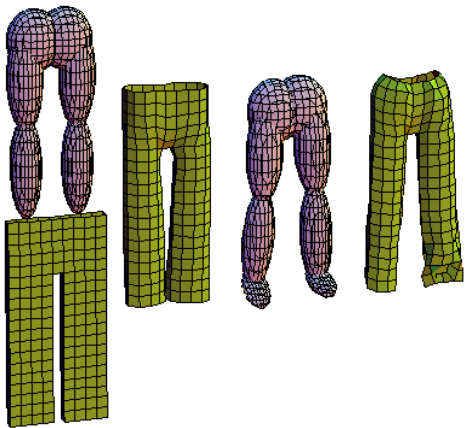

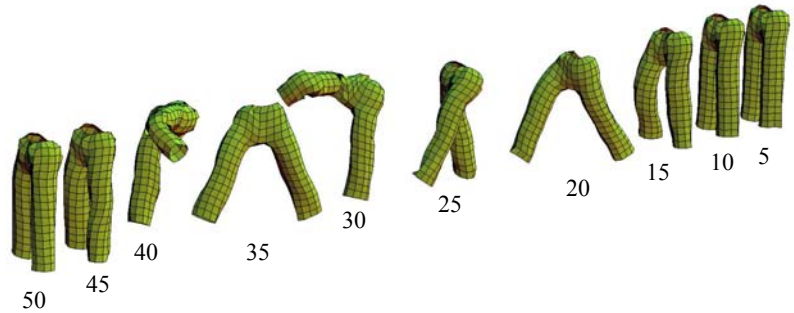Fig. 7. Sequence for the human model to don a pair of pants.

Fig.8: Simulation of pants interacting with lower body striding and then stepping over an obstacle. Numbers below each figure indicate the frame number of the simulation (c.f. Fig. 10).

To quantify the interaction between the pants and the legs, the contact forces were completely available. At any instant in time, the torque (Fig. 9) exerted on a joint is computed as follows: $\tau = \Sigma_{i \in AJ} (\mathbf{x}_i - \mathbf{J}) \times \mathbf{f}_i$ where: $\mathbf{x}_i$ is the position of a clothing node/particle; $\mathbf{f}_i$ is the nodal contact force exerted by the clothing on the body; $\mathbf{J}$ is the instantaneous coordinate of the joint center and AJ is the set of nodes/particles that contribute to the torque on the joint J under consideration. The composition of AJ needs further study to determine which portions of the clothing exert meaningful torque on each joint. The computed torques about the right knee for both stiff and compliant pants are shown in Fig. 10.
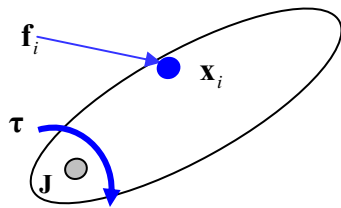

Fig. 9. Computation of instantaneous torques exerted by the clothing about the joint centers.
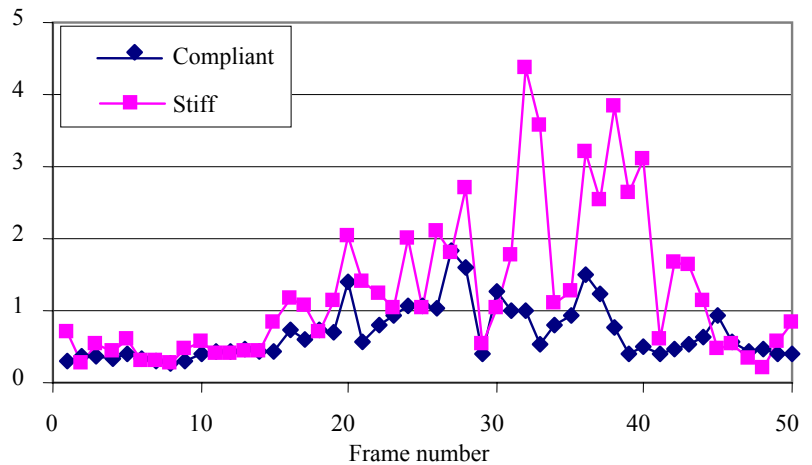

Fig. 10. Computed joint torques about the right knee exerted by the clothing.

5. DISCUSSION

A modeling framework has been presented for quantifying the resistance a given clothing system design will exert on a human model of a specified anthropometry performing a specific task, with the associated kinematics measured via motion capture. In the current framework, the anthropometry of the human is modeled rather approximately using rigid ellipsoidal segments. Both the assumption of rigidity of body segments and the assumption of ellipsoidal geometry to represent body segments can be generalized.

In the current examples, the motion of the human model is fully prescribed. It is realized that if the clothing system exerts significant resistance on the wearer tasked to perform a certain task, the wearer might actually change their strategy for accomplishing the task to reduce the clothing resistance. Although such effects are not captured in the current framework, this is one of the key objectives of our research effort to develop autonomous digital human models that can indeed adapt to the resistance they experience.

Two alternative macroscale fabric modeling techniques have been implemented and tested in our clothing modeling framework: The first is a particle-based method which begins with a discrete treatment of the fabric as a system of springs and masses. By experimenting with the spring stiffnesses and masses in such a modeling framework, simulations of clothing that appear visually realistic can be achieved. However, if the objective of the modeling is to realistically quantify the mechanical resistance that the clothing exerts on the wearer, visual realism alone will not be sufficient. For this reason, the continuum degenerated shell formulation implemented and tested in the current framework is somewhat more attractive to the authors. Specifically, one can insert realistic constitutive material models for fabrics and/or body armor segments into the continuum shell framework thereby increasing the likelihood of calculating more realistic mechanical resistance parameters. Indeed, mechanical realism is paramount in a clothing modeling framework used in designing protective systems for defense and security applications.   Due to the relative simplicity of the spring-mass particle method used herein, it might be especially useful to get the clothing system properly positioned on or donned by the digital human model. However when the real activity of vital interest is performed, the framework can then switch over to the more realistic continuum shell treatment of the clothing.

6. ACKNOWLEDGEMENTS

REFERENCES

1. Bathe, K.J. *Finite Element Procedures in Engineering Analysis*, Prentice-Hall, Englewood Cliffs, NJ, 1982.
2. Belytschko, T., Liu, W.K. and Moran, B. *Nonlinear Finite Elements for Continua and Structures*, John Wiley & Sons, Ltd., 2000.
3. Benson, D.J. and Hallquist, J.O. "A single surface contact algorithm for the post-buckling analysis of shell structures," *Computer Methods in Applied Mechanics and Engineering*, 78: 141-163, 1990.
4. Breen, D.E., House, D.H. and Wozny, M.J. "A particle-based model for simulating the draping behavior of woven cloth," *Textile Research Journal*, 64(11): 663-685, 1994
5. Breen, D.E., House, D.H. and Wozny, M.J. "Predicting the drape of woven cloth using interacting particles," *Computer Graphics* (*Proc. SIGGRAPH*), 365-372, 1994.
6. Carignan, M., Yang, Y., Thalmann, N.M. and Thalman, D. "Dressing animated synthetic actors with complex deformable clothes," *Computer Graphics*, 26(2): 99-104, 1992.
7. Chen, B. and Govindaraj, M. "A physically based model of fabric drape using flexible shell theory," *Textile Research Journal*, 65(6): 324-330, 1995.
8. Chen, B. and Govindaraj, M. "A parametric study of fabric drape," *Textile Research Journal*, 66(1): 17-24, 1996.
9. Choi, K. and Ko, H. "Stable but responsive cloth," In *Computer Graphics* (*Proc. SIGGRAPH*), 604-611, 2002.

10. Chu, G.C., Cummings, C.L. and Teixeira, N.A. "Mechanics of elastic performance of textile materials, Part V: A study of the factors affecting the drape of fabrics – The development of a drape meter," *Textile Research Journal*, 20: 539-548, 1950.
11. Collier, J.R., Collier, B.I., O'Toole, G. and Sargand, S.M. "Drape prediction by means of finite-element analysis," *Journal of the Textile Institute*, 82(1): 96-107, 1991.
12. Cusick, G.E. "The measurement of fabric drape," *Journal of the Textile Institute*, 59(6): 253-260, 1968.
13. Eberhardt, B., Weber, A. and Strasser, W. "A fast, flexible, particle-system model for cloth draping," *IEEE Computer Graphics and Applications*, 16(5): 52-59, 1996.
14. Eischen, J.W. Deng, S. and Clapp, T.G. "Finite-element modeling and control of flexible fabric parts," *IEEE Computer Graphics and Applications*, 16(5): 71-80, 1996.
15. Eringen, A.C.E. *Mechanics of continua*, Krieger, 1981.
16. Gan, L., Ly, N.G. and Steven, G.P. "A study of fabric deformation using nonlinear finite elements," *Textile Research Journal*, 65(11): 660-668, 1995.
17. Govindaraju, N.K., Knott, D., Jain, N., Kabul, I., Tamstorf, R., Gayle, R., Lin, M.C. and Manocha, D. "Interactive collision detection between deformable models using chromatic decomposition," *Proc. of ACM SIGGRAPH*, 24(3): 991-999, 2005
18. Hallquist, J.O., Goudreau, G.L. and Benson, D.J. "Sliding interfaces with contact-impact in large-scale Lagrangian computations," *Computer Methods in Applied Mechanics and Engineering*, 51: 107-137, 1985.
19. Hughes, T.J.R. *The Finite Element Method Linear Static and Dynamic Finite Element Analysis*, Prentice-Hall, Inc., Eaglewood Cliffs, NJ, 1987.
20. Kawabata, S. *The Standardization and Analysis of Hand Evaluation* (The Textile Machinery Society of Japan, Osaka, 1980).
21. Laursen, T.A. and Simo, J.C. "A continuum-based finite element formulation for the implicit solution of multibody, large deformation frictional contact problems," *International Journal for Numerical Methods in Engineering*, 36: 3451-3485, 1993.
22. Provot, X. "Deformation constraints in a mass-spring model to describe rigid cloth behavior," *Proc. Graphics Interface*, 147-154, 1995.
23. Rahmatalla, S., Kim, H., Shanahan, M. and Swan, C.C. "Effect of restrictive clothing on balance and gait using motion capture and dynamic analysis," Paper# 2005-01-2688, *SAE 2005 Transactions Journal of Passenger Cars-Electronic and Electrical Systems*, March 2006
24. Riks, E. "The application of Newton's method to the problem of elastic stability," *Journal of Applied Mechanics*, 39:1060-1065, 1972.
25. Simo, J.C. and Fox, D.D. "On a stress resultant geometrically exact shell model. Part I: Formulation and optimal parameterization," *Computer Methods in Applied Mechanics and Engineering*, 72: 267-304, 1989
26. Simo, J.C., Fox, D.D. and Rifai, M.S. "On a stress resultant geometrically exact shell model. Part II: The linear theory; computational aspects," *Computer Methods in Applied Mechanics and Engineering*, 73: 53-92, 1989.
27. Simo, J.C., Fox, D.D. and Rifai, M.S. "On a stress resultant geometrically exact shell model. Part III: Computational aspects of the nonlinear theory," *Computer Methods in Applied Mechanics and Engineering*, 79: 21-70, 1990.
28. Simo, J.C. and Laursen, J.C. "An augmented Lagrangian treatment of contact problems involving friction," *Computers and Structures*, 42: 97-116, 1992.
29. Spencer, A.J.M. *Continuum Theory of The Mechanics of Fiber-Reinforced Composites*, Springer Verlag, 1984.
30. Swan, C.C. and Cakmak, A.S. "A hardening orthotropic plasticity model for pressure insensitive composites: continuum formulation and integration algorithm," *International Journal for Numerical Methods in Engineering*, 37: 839-860, 1994.
31. Swan, C.C. and Kosaka, I. "Homogenization-based analysis and design of composites," *Computers and Structures*, 64: 603-621, 1997.
32. Terzopoulos, D., Platt, J., Barr, A. and Fleischer, K. "Elastically deformable models," *Computer Graphics* (*Proc. SIGGRAPH*), 21(4): 205-214, 1987.
33. Terzopoulos, D. and Fleischer, K. "Modeling inelastic deformation: viscoelasticity, plasticity, fracture," *Computer Graphics*, 22(4): 269-278, 1988.